Environ. Sci. Technol. **2002**, *36,* 4162−4169

Impact of Surface Heterogeneity on Mercury Uptake by Carbonaceous Sorbents under UHV and Atmospheric Pressure

S. KWON,[†,‡] E. BORGUET,[‡,§] AND R. D. VIDIC*[,†]

Department of Civil and Environmental Engineering, Surface Science Center, and Department of Chemistry, University of Pittsburgh, Pittsburgh, Pennslyvania 15261

Chemical and morphological heterogeneities of carbon sorbents play important roles in gas-phase adsorption. However, the specific chemical complexes and topological structures of carbon that favor or impede elemental mercury uptake are not well understood and are the subject of this study. Temperature programmed desorption (TPD) with a model carbonaceous material (highly oriented pyrolytic graphite, HOPG) under ultrahigh vacuum (UHV) conditions and fixed bed adsorption by activated carbon (BPL) at atmospheric pressure were combined to investigate the effects of chemical and morphological heterogeneities on mercury adsorption by carbonaceous surfaces. TPD results show that mercury adsorption at 100 K onto HOPG surfaces with and without chemical functional groups and topological heterogeneity created by plasma oxidation occurs through physisorption. The removal of chemical functionalities from the HOPG surface enhances mercury physisorption. Plasma-oxidation of HOPG provides additional surface area for mercury adsorption. However, the pits created by plasma oxidation are more than 10 nm in diameter and do not simulate microporosity that predominates in activated carbons. Mercury adsorption by activated carbon at atmospheric pressure occurs through two distinct mechanisms. Physisorption governs mercury adsorption at lower temperatures (i.e., below 348 K), while chemisorption predominates at high adsorption temperatures (i.e., above 348 K). Presence of water on activated carbon surface enhances mercury uptake by both physisorption and chemisorption. Oxygen containing functional groups reduce mercury uptake by physisorption by blocking access to the micropores. No significant impact of oxygen functionalities was observed in the chemisorption regime. The key findings of this study open the possibility to apply scientific information obtained from the studies with simple surfaces such as HOPG under ideal conditions (UHV) to industrial sorbents under realistic process conditions.

Introduction

Environmental control agencies, researchers, and the general public have raised serious concerns about the mobilization and release of trace elements to the environment from fossil fuel burning and various combustion processes (i.e., municipal, medical, and hazardous waste incineration) due to their impact on environment and human health. Mercury is a trace element of special concern because its high volatility allows transfer into the flue gas stream during combustion. Once emitted to the environment, mercury can be deposited locally or globally to create a long-term contamination problem (*1, 2*). Mercury compounds have long been recognized as very potent neurotoxins. Mercury vapor is a nonpolar monatomic gas that is highly soluble in cell membranes (*3*). It is, therefore, efficiently absorbed in the lung and rapidly transported to all target organs, e.g., brain and kidneys (*3*).

The U.S. Environmental Protection Agency (EPA) estimated mercury emissions from coal-fired power plants (CFPP), commercial or industrial boilers, and municipal solid waste incinerators (MSWI) at about 100 tons per year, which represents 65% of total anthropogenic mercury emissions in the United States (*4*). Many countries have established limits on the emissions of hazardous air pollutants. The EEC (European Economic Community) is restricting mercury emissions from municipal waste incinerators to 50 $\mu g/m^3$ based on 11% oxygen (O_2) (*5*). Most states in the U.S. have imposed mercury emission limits for MSWI in the range of 100−130 $\mu g/m^3$ at 7% oxygen (O_2) (*5*). EPA has announced its intention to promulgate regulations for mercury emissions from coal-fired power plants by 2004 and to enforce them by 2007.

Activated carbon adsorption is a unit process that offers great promise for achieving high quality air emissions with respect to mercury and other trace elements that are emitted from coal-fired power plants and other combustion process (*6*). Based on the success of powdered activated carbon (PAC) injection to control trace emissions from MSWIs (*7*, *8*), the same mode of activated carbon application is currently favored for CFPPs due to low capital costs associated with this technology and considerable experience in the utility industry. There are significant differences between the relevant process conditions at CFPPs and MSWIs that preclude direct transfer of the experience with PAC injection technology. For example, the mercury concentration in the flue gas of an MSWI is 1 or 2 orders of magnitude greater than that in CFPPs. Also, the temperature and composition of the flue gas (e.g., HCl, SO_x, and NO_x concentration) are quite different for the two combustion processes (*9*). In addition, most of the mercury in MSW is present in its oxidized form, while a significant portion of mercury emissions from CFPPs is in the elemental form (*10, 11*).

While there are numerous factors that can influence mercury removal by PAC injection, sorbent properties are likely to be among the most important. However, the impact of chemical (e.g., acidity, basicity, functional groups) and physical (e.g., pore size distribution, pore volume, surface area, ...) properties of the carbon surface on mercury uptake are not well understood. This is mostly due to the fact that complex pilot-scale studies under realistic process conditions incorporate many factors (e.g., flue gas composition, temperature, contact time) that may influence mercury removal by PAC (*9*, *12*, *13*). It is now clear that the development of efficient and cost-effective sorbents must be based on fundamental understanding of adsorption mechanisms that can only be obtained from well-controlled laboratory studies.

This study compares adsorption and desorption of gas-phase elemental mercury on real and model carbonaceous surfaces in order to provide clear understanding of their

* Corresponding author phone: (412)624-1307; fax: (412)624-0135; e-mail: vidic@engrng.pitt.edu.
† Department of Civil and Environmental Engineering.
‡ Surface Science Center.
§ Department of Chemistry.

10.1021/es0256818 CCC: $22.00
Published on Web 08/23/2002

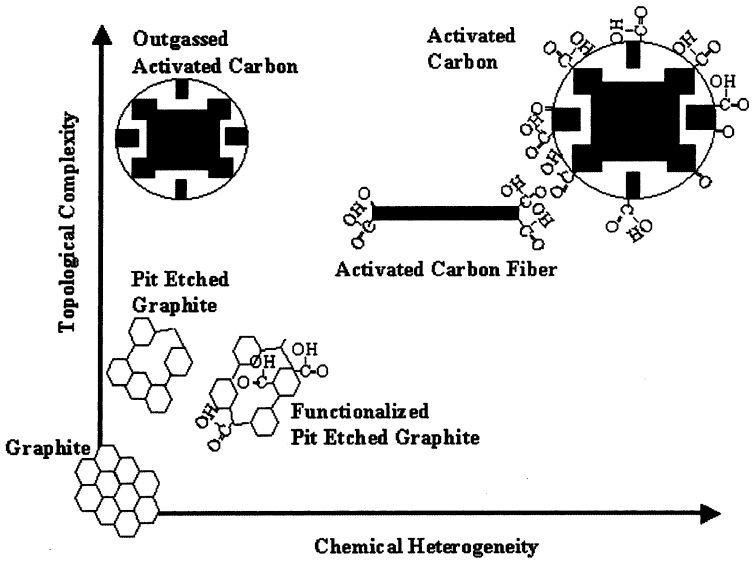

FIGURE 1. Chemical and topological heterogeneity of carbonaceous surfaces used in fundamental laboratory studies and in industrial practice.

interactions. The investigation of elemental mercury adsorption was carried out using highly oriented pyrolytic graphite (HOPG), as a model carbonaceous surface under well-controlled ultrahigh vacuum (UHV) conditions and a coal based activated carbon in fixed-bed configuration. While it is clear that there are major differences between graphite and real carbonaceous sorbents with regards to inorganic impurities (ash content) and morphology, it is possible to modify the pore structure and chemical heterogeneity (surface functional groups) of HOPG to capture the essential features of porous carbons that are believed to be the key surface properties influencing adsorption by carbonaceous sorbents. Carefully selected thermal and chemical modifications of graphite and activated carbon (e.g., etching, oxidation, outgassing) could bridge the differences between these surfaces to reveal key surface properties for adsorption and catalysis and facilitate a better understanding of these mechanisms.

As can be seen in Figure 1, this study represents an important step in trying to overcome vast differences in chemical and topological heterogeneity between a simple surface like HOPG and a complex industrial sorbent like activated carbon. Virgin HOPG is assumed to contain no chemical or topological heterogeneity. Creating pits in this homogeneous surface and decorating the edge atoms with typical oxygen functionalities (e.g., carboxyl, carbonyl, etc.) would impart some of the features that are known to exist on activated carbon (*14*−*16*). On the other hand, there is very little that can be done to alter the topological heterogeneity of activated carbon in a controlled fashion. However, outgassing at elevated temperatures would remove most of the oxygen functionalities on this industrial sorbent with minor changes in surface area, pore structure, or pore size distribution (*17*).

While there is still a significant void space in Figure 1, it should be possible to fill it at least partially through careful selection and modification of other carbonaceous surfaces such as carbon molecular sieves, activated carbon fibers, carbon nanotubes, etc. This study represents the first steps in filling that space in an effort to understand fundamental aspects of elemental mercury adsorption by carbonaceous sorbents.

Experimental Protocols

1. UHV Experiments. A stainless steel ultrahigh vacuum (UHV) chamber was pumped by a turbomolecular pump backed by a mechanical pump to provide a base pressure of 5×10^{-10} Torr after bakeout of the entire chamber for 3 days at around 450 K (*18*). The chamber was equipped with a Bayard-Alpert type nude ion gauge and a quadrupole mass spectrometer (QMS, AccuQuad300, Stanford Research System, Sunnyvale, CA) to measure total and partial pressure in the chamber.

The QMS probe was housed in a stainless steel shield with a 2.5 mm diameter aperture. The QMS and shield assembly can be repeatedly located to within < 1 mm of the sample for temperature programmed desorption (TPD) experiments. This configuration ensures the collection of molecules from the sample surface alone during TPD (*19*). Retraction of the QMS and shield assembly up to 20 mm by a movable bellows device allows for sample rotation and adsorbate exposure.

A custom-made sample holder, depicted schematically in Figure 2, which allows cooling and independent heating of two samples was used in these experiments. This enabled sample comparison under almost identical conditions. The dual sample holder consisted of two pairs of copper supports. The sample holder can be rotated around the *z*-axis by a sample manipulator (Model RMTG-275, MDC, Hayward, CA). A pair of supports was mechanically mounted on each side of a copper block silver soldered to a stainless steel liquid nitrogen reservoir. Each copper support was electrically isolated by a sapphire disk (Meller Optics, Providence, RI) in order to allow individual heating of each sample. Samples were mounted on the copper supports with stainless steel screws and Ta support plates. Samples can be cooled to 88 K with liquid N_2 and resistively heated to 1323 K. K-type thermocouples were spot-welded to the Ta support plates and wedged against each of the samples.

Two $10 \times 10 \times 0.25$ mm HOPG samples (Grade SPI-1, SPI Supplies Co., West Chester, PA) were used to produce air-cleaved HOPG and plasma-oxidized HOPG samples. Air-cleaved HOPG was produced by peeling away topmost layers using Scotch tape. The plasma oxidation was performed for 20 and 90 min in a plasma generator (Super Plasmod, March Inst. Co., Concord, CA) with 1 mbar of O_2 pressure and 100 W of power. Prior to installation in the UHV chamber the samples were imaged by AFM (Pico SPM, Molecular Imaging, Phoenix, AZ) in air using the contact mode.

Research grade mercury, taken from a permeation tube (VICI Metronics, Inc. Santa Clara, CA), was used as a source of mercury vapor in the chamber. Mercury dosing was

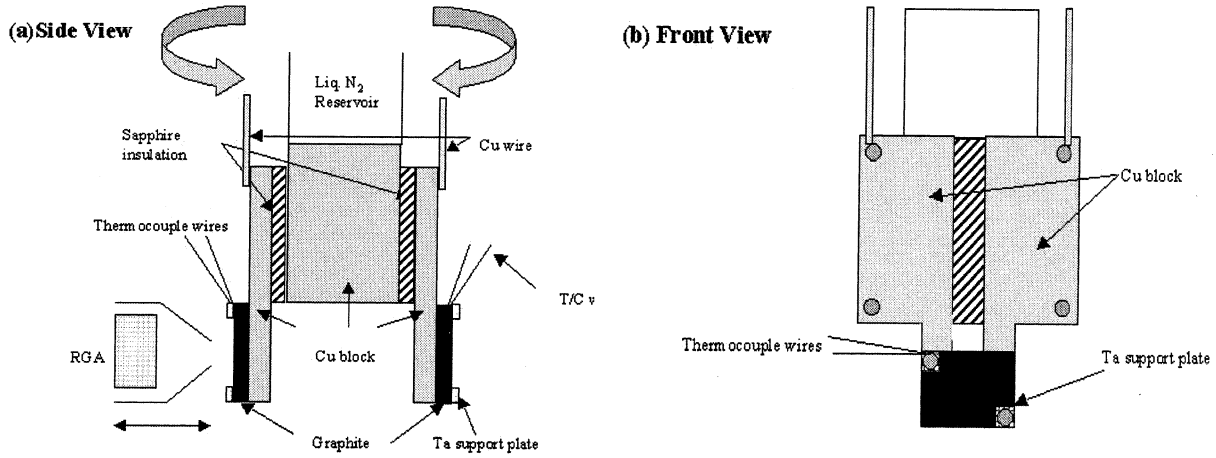

FIGURE 2. Schematic view of the dual sample mount: (a) side view and (b) front view.

performed by backfilling the chamber. To increase the mercury vapor pressure, gas-handling lines were heated to about 360 K for all experiments. Mercury exposures are reported in Langmuir units ($1\ L = 10^{-6}$ Torr s) as determined by uncorrected ion gauge readings.

A constant temperature ramping rate, typically 2.5 K/s, was applied during a TPD experiment, while partial pressure and sample temperature were measured using a personal computer equipped with an A/D board controlled by a customized LabView program (National Instruments, Austin, TX). Mercury pressure during TPD experiments was measured by monitoring the QMS signal at 201 *m*/*e*. The heated sample was observed through a viewport to glow with a uniform color, suggesting that it is uniformly heated.

2. Fixed-Bed Adsorption Experiments. Commercially available coal-based activated carbon, (BPL, Calgon Carbon Corporation, Pittsburgh, PA) was evaluated for vapor-phase elemental mercury uptake using a fixed-bed adsorber. The particle size used in this study was 60 × 80 U.S. mesh size. Prior to charging the adsorber, some activated carbon samples were outgassed by heating to 423 K for 30 min (BPL-423) and 1173 K (BPL-1173) overnight in a nitrogen atmosphere to remove moisture and/or oxygen-containing chemical functional groups (*15*, *16*). The outgassed samples were allowed to cool to room temperature under nitrogen atmosphere and immediately transferred to the reactor to minimize readsorption of oxygen-containing functionalities and avoid contamination that may result from prolonged exposure to ambient laboratory conditions.

Industrial grade nitrogen was used as a carrier gas in all experiments to transport mercury vapor from a permeation tube (VICI Metronics, Inc., Santa Clara, CA) submerged in an oil bath to the adsorber. The flow rate of the carrier gas was controlled by a mass flow controller (Tylan General, Torrance, CA) at 1 L/min, while constant mercury concentrations of 70, 530, 780, and 1120 $\mu g/m^3$ were accomplished by controlling the oil bath temperature.

Fixed-bed adsorber experiments were performed at 293, 323, 348, 383, and 423 K using a quarter inch diameter stainless steel column charged with 100 mg of sorbent. The adsorber was placed in a laboratory oven (Cole Parmer Instrument Company, Niles, IL) to control the temperature of adsorption. To facilitate efficient heating of the influent gas, 4 ft of coiled Teflon tubing was installed in the oven prior to the adsorber inlet. An atomic absorption spectrophotometer (Model 403, Perkin-Elmer, Norwalk, CT) equipped with an 18-cm hollow quartz cell (Varian Australis Pty, Ltd., Mulgrave, Victoria, Australia) was used to continuously measure the concentration of vapor-phase elemental mercury in the effluent stream. Quality control procedures used in this study were identical to those described by Korpiel and Vidic (*20*) and resulted in negligible adsorption of mercury onto the tubing and stainless steel, isothermal operation of the reactor system, accurate mass balance for mercury in each experiment, and the absence of oxidized mercury species in the reactor effluent.

Results and Discussion

1. TPD for Virgin HOPG. Air cleaved HOPG contains significant amounts of oxygen containing functional groups that can be removed by thermal treatment over 500 K (*21*). A series of TPD experiments was carried out to investigate the impact of oxygen-containing functional groups on mercury adsorption and desorption from virgin and chemical functional group free HOPG surfaces. TPD spectra for mercury dosed at 100 K on air cleaved HOPG sample following heat treatment to 473 K are shown in Figure 3(a) and to 1273 K in Figure 3(b). A mercury TPD desorption peak appears around 200 K in both cases. It increases in height and width with increasing exposure levels. The peak did not saturate in the exposure range of our experiments, and its location tends to shift to higher temperature with increasing exposure.

The energy of mercury desorption from HOPG can be determined through the analysis of the desorption rate ($-d\theta/dT$), which is commonly described by eq 1 (*22*)

$$-\frac{d\theta}{dT} = \frac{\nu}{\beta}\theta^n \exp\left(-\frac{E_d(1-\alpha\theta)}{RT}\right) \qquad (1)$$

where ν is the preexponential factor, θ is the adsorbate coverage, β is the temperature ramping rate (dT/dt), n is the order of the desorption process, E_d is the heat of adsorption at zero coverage, and α is the intermolecular interaction parameter (positive values of α reflect repulsive intermolecular interactions and negative values of α reveal attractive intermolecular interactions) (*22*, *23*). The experimental TPD spectra can be simulated as illustrated in Figure 4 for the case of mercury exposure at 20L for a 1273 K treated air cleaved HOPG sample. The best fit of eq 1 to all experimental data shown in Figure 3 was obtained using first-order reaction, a preexponential factor of $10^{18\pm1}\ s^{-1}$, an average heat of adsorption of 81 ± 3 kJ/mol, and an intermolecular interaction parameter of -0.003 monolayer^{-1}. Uncertainties arise in part from the accuracy of temperature measurements because the location of the thermocouple is restricted by the fact that it cannot be spot-welded to HOPG. The tailing of the experimentally measured peak at higher temperatures is attributed to the slow pumping speed of Hg in these experiments. The calculated activation energy is about 25% greater than the heat of sublimation of mercury of 64.4 kJ/

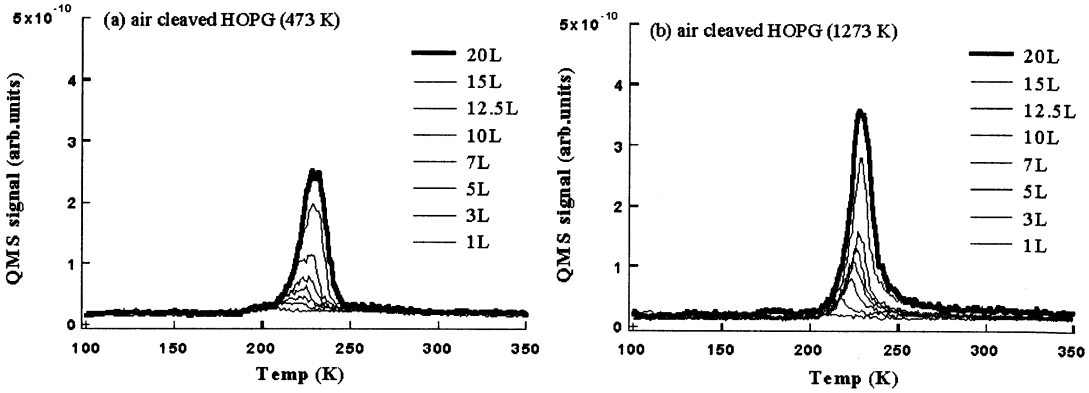

FIGURE 3. TPD spectra of mercury on air cleaved HOPG that was previously heated at (a) 473 K and (b) 1273 K. Spectra are shown for increasing exposure, from 1L to 20L.

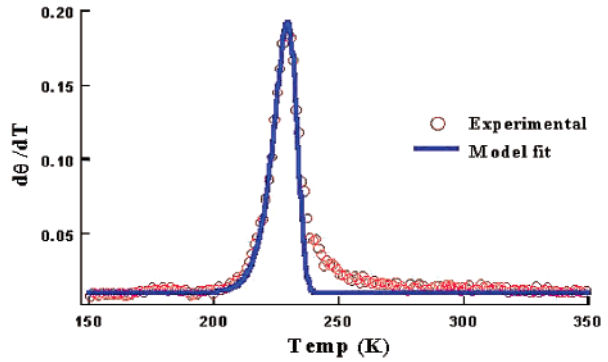

FIGURE 4. Modeling of TPD spectrum at 20 L exposure using coverage dependent first-order desorption kinetics using eq 1 with $\alpha = -0.003$ monolayer^{-1}, $E_d = 81 \pm 3$ kJ/mol, and $\nu = 10^{18\pm1}$ s^{-1}.

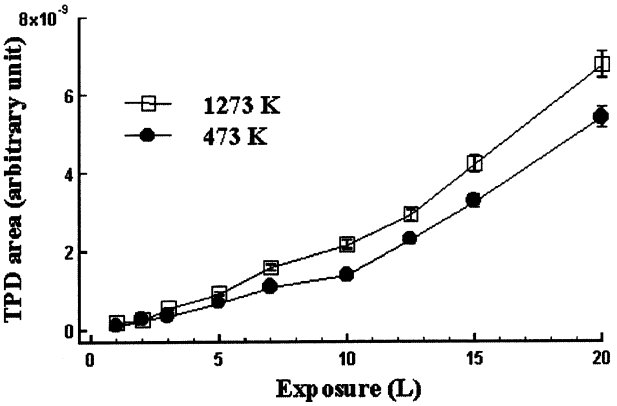

FIGURE 5. TDP area as a function of mercury exposure for air cleaved HOPQ sample heat treated to 473K (●) and 1273 K (□).

mol at 200 K (*24*, *25*). It can be concluded that mercury adsorption on virgin and outgassed HOPG occurs exclusively through physisorption under the experimental conditions used in this study (*26*).

Figure 5 illustrates the integrated TPD areas, which correspond to the relative amount of adsorbed mercury, as a function of mercury exposure for both HOPG samples. These results indicate that the heat treatment of HOPG at 1273 K causes some increase in the amount of mercury adsorbed under the experimental conditions used in this study. Previous studies demonstrated that heat treatment of HOPG leads to desorption of oxygen containing functional groups at temperatures above 500 K and that there is no reappearance of these functionalities over a 24 h period that elapses between successive heat treatments in UHV (*21*). Similar behavior was reported earlier for graphitized carbon fiber (*27*) and activated carbon (*28*), which demonstrated that outgassing above 1273 is required to remove essentially all functional groups. Therefore, it can be concluded that the increase in mercury adsorptive capacity of HOPG after 1273 K heat treatment was caused by the removal of chemical functionalities from the surface. Similar behavior was observed for the adsorption of propane on HOPG (*21*) and xenon on single wall carbon nanotubes (*29*, *30*). Propane, a nonpolar organic, has unfavorable interactions with functional groups that exist on air-cleaved HOPG (*21*). Heating to 1273 K removed these functionalities and resulted in over an order of magnitude increase in adsorption capacity of a nonpolar alkane, propane (*21*). However, the amount of acetone, a polar organic, adsorbed on HOPG is independent of surface heat treatment and depends only on total exposure (*18*). Thermal treatment of HOPG allows acetone molecules to adsorb directly on the HOPG surface (*31*). The increase in mercury adsorption capacity upon heating HOPG to 1273 K was significantly lower, indicating weaker interactions between mercury and the surface functional groups that observed for nonpolar organic adsorbents. It is likely that the chemical functional groups on the HOPG surface are polar (e.g., quinone or carboxylic acid) and that adsorption of a nonpolar organic (e.g., propane) could be hindered by their presence. These chemical functionalities on HOPG still provide adsorption sites for polar species (acetone) and mercury. This is consistent with the well-known imiscibility of polar and nonpolar solvents, e.g., oil and water.

2. TPD for Plasma-Oxidized HOPG. An important objective of this study was to understand the role of topological heterogeneity on the adsorption and desorption on HOPG surfaces under UHV conditions. To introduce defect sites and etch pits on HOPG, an air-cleaved HOPG sample was subjected to plasma treatment at controlled oxygen pressure. It has been shown that high-temperature oxidation in air creates a low density (<1% by surface area) of monolayer deep etch pits at existing defects of HOPG, while maintaining the flatness of the graphite surface (*32*−36). Plasma oxidation, however, creates damage on initially flat surface that augments preexisting defect sites (*35*). Plasma oxidation etches the surface, resulting in highly roughened surfaces as confirmed by AFM measurements (*35*). AFM images of plasma-oxidized HOPG acquired in air before mounting the samples in the UHV chamber are shown in Figure 6. The air-cleaved HOPG (Figure 6(a)) shows a clean and flat surface except for steps of ∼2.5 nm height. A significant density of defects (dark spots in Figure 6(b)) is observed on the 20 min plasma-oxidized HOPG surface. Most defects are around 100 nm in diameter and from ∼1 to ∼10 nm in depth. Plasma oxidation clearly results in the formation of a topologically heterogeneous surface distinct from the topologically homogeneous air-cleaved surface. Longer exposure to plasma

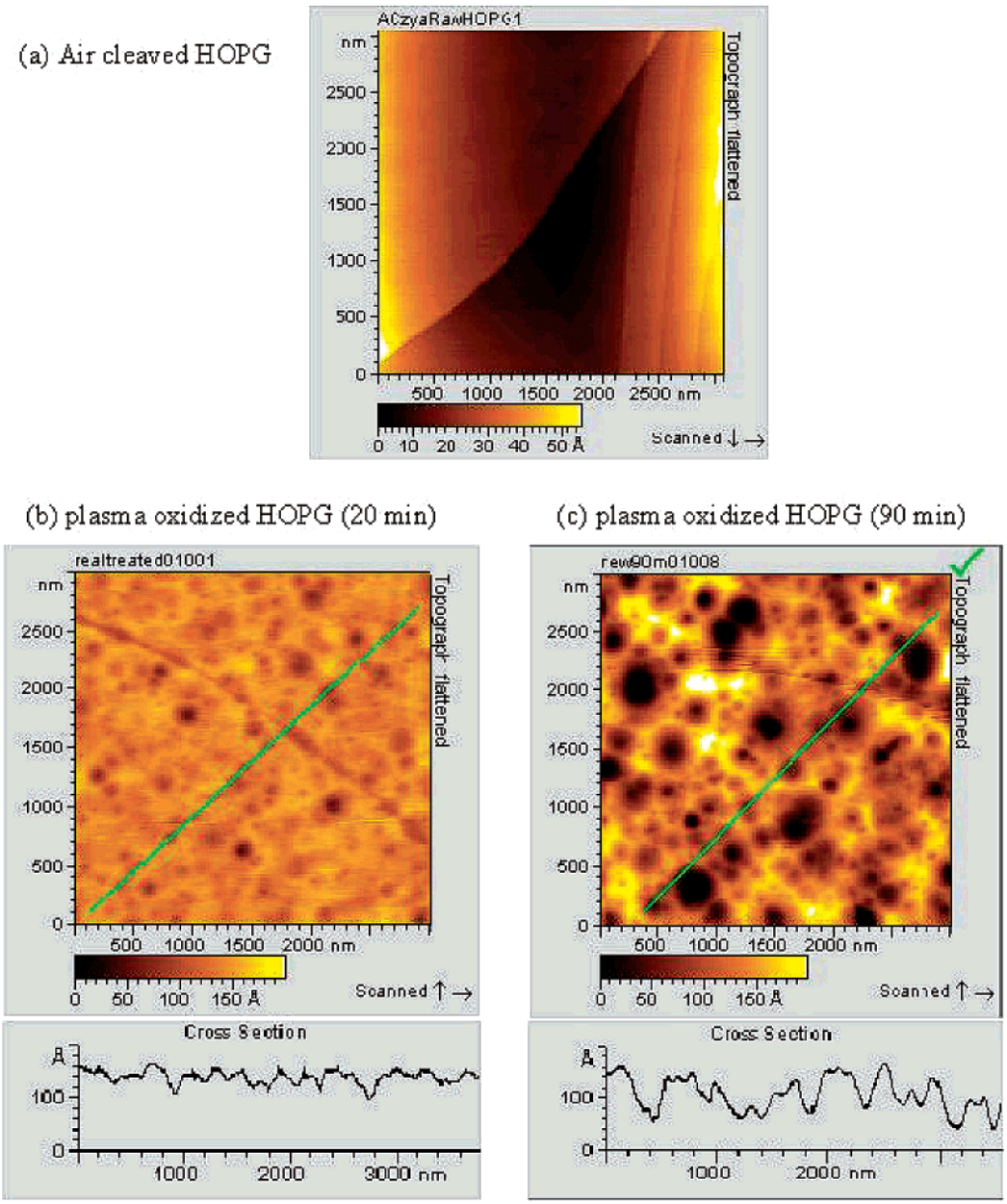

FIGURE 6. AFM images of different HOPG samples: (a) air cleaved, (b) plasma-oxidized for 20 min, and (c) plasma-oxidized for 90 min.

oxidation, for example 90 min (Figure 6(c)), leads to an increase in defect diameter (from ~100 to 500 nm) and depth (from 5 to 20 nm). Similar behavior was reported by Paredes et al. (*35*).

The 20 and 90 min plasma-oxidized HOPG samples were subjected to heat treatment at 1273 K before mercury exposure to ensure that they contain no chemical functionalities and that only the impact of topological heterogeneity on mercury uptake can be studied. Figure 7 shows a series of TPD spectra for mercury dosed at 100 K on plasma-oxidized HOPG, while Figure 8 compares the relative amounts of mercury adsorbed on virgin and plasma-oxidized samples.

The impact of topological heterogeneity on elemental mercury adsorption can be evaluated by comparing TPD spectra for 1273 K treated air cleaved HOPG (Figure 3(b)) to those shown in Figure 7. The changes in the TPD spectra resulting from the difference in topology caused by plasma oxidation are minor. There is no evidence that the defect sites caused by plasma treatment created new adsorption sites for mercury under the experimental conditions used in this study because all desorption peaks appear at almost identical temperature. In addition, the heat of adsorption on plasma-oxidized samples, which was also estimated using coverage dependent first-order kinetics, is within the range of the heat of adsorption determined for air cleaved HOPG sample. As shown in Figures 7 and 8, mercury adsorption capacity of HOPG increased after 20 min plasma oxidation, but no significant increase in the capacity was observed with further oxidation. Therefore, it can be concluded that defect sites created by plasma oxidation only provided additional surface area for mercury adsorption.

On the other hand, the adsorption mechanism for an organic adsorbate (propane) was drastically different for air-cleaved and plasma-oxidized HOPG (*21*). Plasma-created defects provided adsorption sites with stronger binding energy and faster adsorption kinetics for propane molecules as indicated by the appearance of the high-temperature peak in the TPD spectra, the sequence of peak growth in the TPD spectra, and additional adsorption capacity.

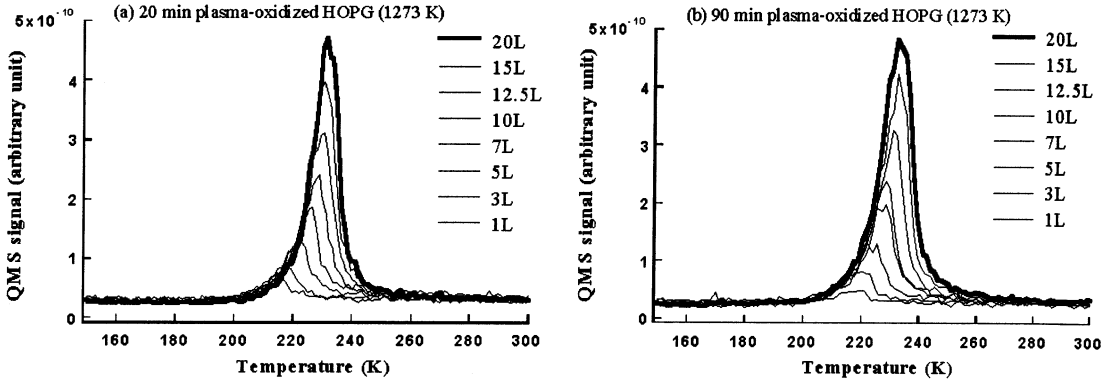

FIGURE 7. TPD spectra of mercury on (a) plasma-oxidized HOPG for 20 min and (b) plasma-oxidized HOPG for 90 min. Note that both HOPG samples were pretreated at 1273 K and that identical scales are used for both figures. Spectra are shown for increasing exposure from 1L to 20L.

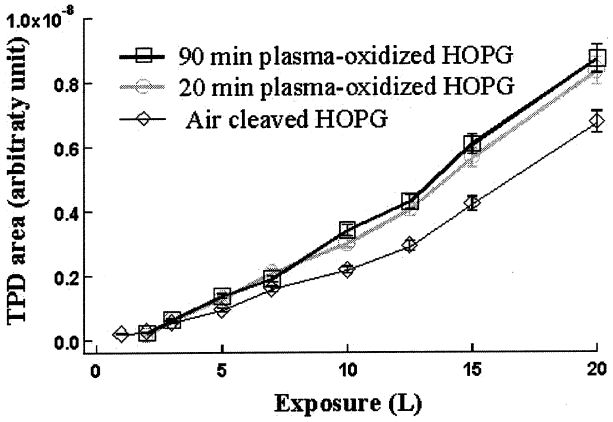

FIGURE 8. TPD area as a function of mercury exposure for air cleaved HOPG, 20 minute plasma-oxidized HOPG, and 90 minute plasma-oxidized HOPG samples after 1273 K heat treatment.

The AFM analyses of plasma-oxidized HOPG did not reveal the presence of micropores (pores below 2 nm in diameter) or mesopores (2−50 nm) on either 20 or 90 min plasma-oxidized HOPG. Although the 90 min plasma-oxidized HOPG had a somewhat larger surface area and a greater number of pits (macropores) created after prolonged exposure to oxygen plasma, it had virtually identical capacity for mercury uptake. It can therefore be concluded that these macropores are not responsible for the majority of mercury uptake and that the sorbents with meso and microporosity should be better suited for mercury adsorption (*37*). The results of all the TPD experiments clearly demonstrated that mercury adsorption at 100 K on HOPG surfaces, with and without chemical functional groups and topological heterogeneity created by plasma oxidation, occurs through physisorption. The removal of oxygen containing functionality from the HOPG surface increases the adsorption capacity, without significant change in adsorption energetics under UHV conditions.

3. Fixed-Bed Adsorption Studies. Breakthrough curves for elemental mercury from an adsorber charged with outgassed BPL carbon measured at different adsorption temperatures and influent mercury concentrations of 70 and 1120 $\mu g/m^3$ are shown in Figure 9. It can be seen that mercury uptake increases with a decrease in the reaction temperature, which follows the well-documented impact of temperature on adsorption (*26*). Breakthrough studies with influent mercury concentrations of 540 and 780 $\mu g/m^3$ were also performed in this study (data not shown here). Mercury uptake as a function of equilibrium vapor pressure at 100% breakthrough, which was determined by integrating breakthrough curves at different bed, temperatures is shown in Figure 10.

It can be observed that the mercury adsorptive capacity increases linearly with an increase in influent mercury concentration for all adsorption temperatures, which suggests that under the experimental conditions used in this study, mercury adsorption on activated carbon occurs in Henry's law region (*26*). Such behavior can be explained by the fact that the highest mercury concentration used in breakthrough experiments was less than 5% of the saturation vapor pressure

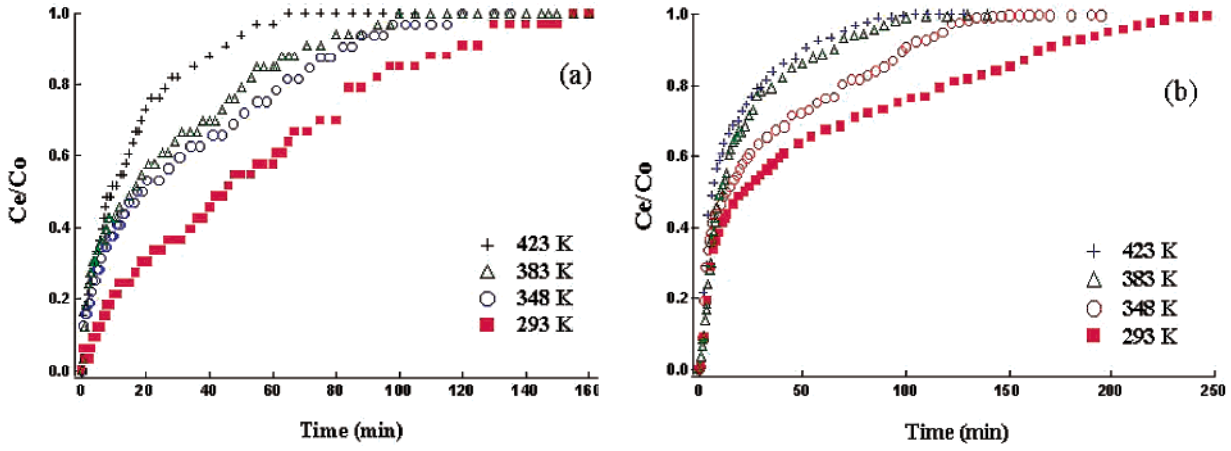

FIGURE 9. Impact of temperature on mercury breakthrough from a fixed bed adsorber at influent mercury concentrations of (a) 70 $\mu g/m^3$ and (b) 1120 $\mu g/m^3$.

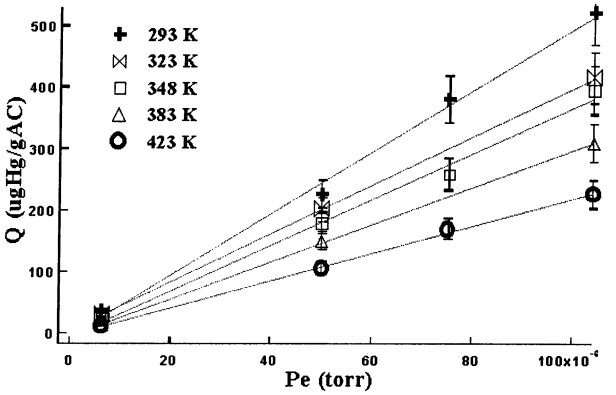

FIGURE 10. Mercury uptake capacity as a function of equilibrium pressure at different reaction temperatures (lines represent linear regression fit to experimental data).

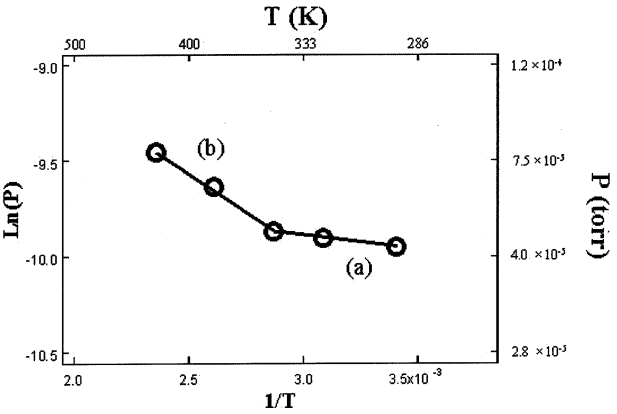

FIGURE 11. Equilibrium pressure at 200 μgHg/gAC as a function of 1/T. Line (a) represents a linear fit to adsorption data collected below 348 K and line (b) is a linear fit to adsorption data collected above 348 K.

at that temperature. In that case, mercury atoms are isolated from their neighbors and the equilibrium relationship between the gas phase and adsorbed phase is linear (*26*).

The adsorption isotherms in Figure 10 can be used to estimate the heat of adsorption of mercury on activated carbon. The relationship between the mercury equilibrium pressure and reaction temperature at constant coverage can be approximated by the Clausius−Clapeyron equation given below

$$\frac{d(\ln P)}{d(1/T)} = -\frac{\Delta H}{R} \qquad (2)$$

where ΔH is the heat of adsorption and R is the ideal gas law constant (*38*).

Figure 11 depicts adsorption equilibrium data in the form of lnP versus $1/T$ for constant coverage of 200 μg/g at different adsorption temperatures investigated in this study. In a first approximation, the experimental data can be divided into two distinct regions with 348 K as the common point. The linear fit to the data collected below 348 K is obtained with the heat of adsorption of 97 ± 5 kJ/mol, while the data collected above 348 K revealed the heat of adsorption of 579 ± 20 kJ/mol. Compared to the heat of vaporization of mercury at 298 K of 66.8 kJ/mol (*24*, *25*), it is clear that the increase in adsorption temperature leads to an increase in the heat of adsorption and a shift from a physisorption to a chemisorption mechanism (*26*). These findings are supported by previous studies that suggested which mercury adsorption by activated carbon occurs through a combination of chemisorption and physisorption at ambient temperature (*9*) and that chemisorption predominates at higher temperatures (*5*, *39*). The heat of adsorption of mercury on activated carbon at low temperatures (below 348 K) is in good agreement with the value of 81 ± 3 kJ/mol estimated from the TPD studies with HOPG at UHV conditions. It can, therefore, be concluded that UHV studies with simple model carbonaceous surface, e.g., HOPG, can be used to investigate mercury adsorption on activated carbon in the physisorption region.

The data presented in Figures 3 and 5 demonstrated extremely limited impact of chemical functional groups on mercury uptake by HOPG. The impact of activated carbon surface chemistry on mercury uptake was studied using fixed-bed adsorption experiments with different samples of BPL activated carbon. Mercury breakthrough was measured for virgin (as received) BPL carbon and BPL carbon that was outgassed at 423 K (BPL-423) and 1173 K (BPL-1173). The heat treatment at 423 K was chosen because the water present on the carbon surface can be removed by this low temperature treatment without changing or damaging the morphological structure of activated carbon (*40*) or removing the significant amount of oxygen containing functional groups that are normally stable up to 473 K (*16*). The heat treatment at 1173 K was chosen in an attempt to completely remove oxygen-containing functional groups from the carbon surface (*17*).

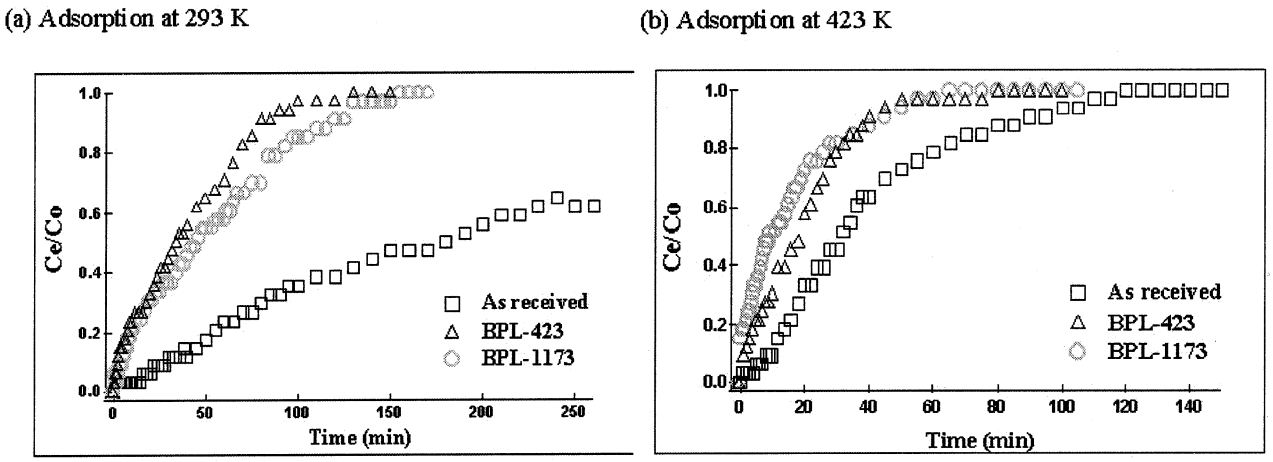

FIGURE 12. Impact of sample pretreatment on elemental mercury breakthrough from a fixed bed adsorber operated at (a) 293 K and (b) 423 K with influent mercury concentration of 70 μg/m^3.

Figure 12 compares mercury breakthrough at 293 and 423 K from fixed-bed adsorbers charged with different BPL samples using influent mercury concentration of 70 $\mu g/m^3$. The operating temperatures of 293 and 423 K were selected based on the findings shown in Figure 11 to facilitate physisorption and chemisorption mechanisms for mercury uptake, respectively. Breakthrough profiles in Figure 12 (parts (a) and (b)) suggest that the virgin BPL sample with original moisture content had the highest mercury adsorption capacity among the samples tested in this study. This observation agrees with the findings of Li et al. (*41*), who also suggested that the surface water content of a carbon-based sorbent significantly enhances mercury uptake. However, the water content was less significant for mercury uptake in the chemisorption region because water is vaporized and removed from the carbon surface during the adsorption experiment at high bed temperatures. Figure 12(a) also shows that mercury uptake capacity in the physisorption region increases by about 25% as a result of the removal of surface functional groups by outgassing at 1123 K. A possible explanation for such behavior is that these functional groups restrict access of mercury molecules to micropores that are very important for physisorption as demonstrated in studies with HOPG. On the other hand, removal of surface functionalities has an adverse impact on mercury uptake by chemisorption as shown in Figure 12(b). Such behavior was expected because oxygen containing functional groups are important chemisorption sites for elemental mercury (*42*).

It is important to note here that the observed increase in adsorption capacity of activated carbon in the physisorption region resulting from the removal of chemical functionalities is in agreement with the UHV experiments with HOPG. In addition, these experiments with activated carbon conducted at atmospheric pressure reveal that chemisorption, while providing stronger binding sites, accounts for smaller fraction of the total capacity than the physisorption sites. Furthermore, access to the chemisorption sites appears to be activated, and these sites are only populated in high-temperature atmospheric pressure experiments.

In conclusion, temperature programmed desorption (TPD) of Hg from a model carbonaceous material (highly oriented pyrolitic graphite, HOPG) under ultrahigh vacuum (UHV) conditions was successfully combined with fixed bed adsorption experiments on activated carbon (BPL) at atmospheric conditions to investigate the effects of chemical and morphological heterogeneities on mercury adsorption by carbonaceous surfaces. The key findings of this study open the possibility to apply scientific information obtained from experiments with simple model carbonaceous surfaces under ideal conditions to industrial carbonaceous sorbents under realistic process conditions. HOPG surfaces can be modified chemically and topologically by plasma oxidation to simulate some of the key features of activated carbon adsorbents. The good agreement between the heats of adsorption determined from TPD studies under UHV conditions and breakthrough experiments at atmospheric pressure validates the proposed approach to bridge the traditional pressure gap in surface science (*43*). Further experiments to probe the role of chemical and topological heterogeneity on activated carbon are in progress.

Acknowledgments

This work is supported by the U.S. Department of Energy under Grant No. DE-FG26-98FT40119. We acknowledge Dr. Yufan He for help in obtaining the AFM images and Dr. William R. Wagner and Mr. Brian Fill for assistance in plasma oxidation treatment of HOPG.

Literature Cited

(1) McFarland, R. B.; Reigel, H. *J. Occup. Med.* **1978**, *20*, 532.
(2) Igata, A. *Advances in Mercury Toxicology*, "*Epidemiological and Clinical Features of Minamata Disease*"; Susuki, T., Ed.; Plenum Press: New York, 1991.
(3) Clarkson, T. *Proceedings of the 1993 International Municipal Waste Combustion Conference, Williamsburg, VA;* 1993, p 591.
(4) Brown, T. D.; Smith, D. N.; Hargis, R. A., Jr.; O'Dowd, W. J. *J. AWMA, Critic. Rev.* **1999**, 1.
(5) Krishnan, S. V.; Gullett, B. K.; Jozewicz, W. *Environ. Sci. Technol.* **1994**, *28*, 1506.
(6) Ghorish, B.; Gullett, B. K. *Waste Manag. Res.* **1998**, *16*, 582.
(7) Carey, T. R.; Hargrove, J. W. O.; Richardson, C. F.; Chang, R.; Meserole, F. B. *Proceedings of the 90th Annual Meeting & Exhibition on the Air and Waste Management Association, Toronto, Ontario, Canada*; 1993; p 97.
(8) Sjostrum, S.; Smith, J.; Hunt, T.; Chang, R.; Brown, T. D. *Proceedings of the 90th Annual Meeting & Exhibition on the Air and Waste Management Association, Toronto, Ontario, Canada, 1997 July 8−13, p 97.*
(9) Chang, R.; Offen, G. *Power Eng.* **1995**, *99*, 51.
(10) Billings, C. E.; Sacco, A. M.; Matson, W. R.; Griffin, R. M.; Coniglio, W. R.; Harley, R. A. *J. Air. Pollut. Cont. Assoc.* **1973**, *23*, 773.
(11) Pacyna, J. M.; Munch, J. *Water, Air, Soil Pollut.* **1991**, *56*, 51.
(12) Carey, T. R.; Richardson, C. F.; Hargrove, J. W. O.; Chang, R.; Meserole, F. B. *1999 AIChE Spring National Meeting*; 1999.
(13) Krishnan, S. V.; Gulett, B. K.; Jozevice, W. Presented at *Solid waste management: thermal treatment & waste-to-energy technologies, U.S. EPA/RREL & AWMA, April 18−21, 1995.*
(14) Hall, R. C.; Holmes, R. J. *Carbon* **1992**, *30*, 173.
(15) Hall, R. C.; Holmes, R. J. *Carbon* **1993**, *31*, 881.
(16) Otake, Y.; Jenkins, R. G. *Carbon* **1993**, *31*, 109.
(17) Tessmer, C. H.; Vidic, R. D.; Uranowski, L. J. *Environ. Sci. Technol.* **1997**, *31*, 1872.
(18) Kwon, S.; Russell, J.; Zhao, X.; Vidic, R.; Johnson, J. K.; Borguet, E. *Langmuir* **2002**, *18*, 2595.
(19) Schlichting, H.; Menzel, D. *Surf. Sci.* **1993**, *285*, 209.
(20) Korpiel, J. A.; Vidic, R. D. *Environ. Sci. Technol.* **1997**, *31*, 2319.
(21) Kwon, S.; Vidic, R.; Borguet, E. *Carbon* **2002**, in print.
(22) Paserba, K. R.; Gellman, A. J. *J. Chem. Phys.* **2001**, *115*, 6737.
(23) Redhead, P. A. *Vacuum* **1962**, *12*, 203.
(24) Lide, D. R. *CRC Handbook of Chemistry and Physics*, 78th ed.; CRC Press: Boca Raton, 1997.
(25) Yaws, C. L., Ed. *Chemical Properties Handbook*; McGraw-Hill: New York, 1999.
(26) Ruthven, D. M. *Principles of Adsorption and Adsorption Processes*; John Wiley & Sons: New York, 1984.
(27) Dandekar, A.; Baker, R. T. K.; Vannice, M. A. *Carbon* **1998**, *36*, 1821.
(28) Ma, M. C.; Brown, T. C.; Haynes, B. S. *Surf. Sci.* **1993**, *297*, 312.
(29) Kuznetsova, A.; Mawhinney, D. B.; Naumenko, V.; Yates, J. T., Jr.; Lui, J.; Smalley, R. E. *Chem. Phys. Lett.* **2000**, *321*, 292.
(30) Mawhinney, D. B.; Naumenko, V.; Kuznetsova, A.; Yates, J. T., Jr.; Smalley, R. E. *Chem. Phys. Lett.* **2000**, *324*, 213.
(31) Kwon, S.; Vidic, R.; Borguet, E. **2002**, *submitted to Surf. Sci.*
(32) Chang, H.; Bard, A. J. *J. Am. Chem. Soc.* **1990**, *112*, 4598.
(33) Chang, H.; Bard, A. J. *J. Am. Chem. Soc.* **1991**, *113*, 5588.
(34) Stevens, F.; Kolodny, L. A.; Beebe, T. P. *J. Phys. Chem. B* **1998**, *102*, 10799.
(35) Paredes, J. I.; Martinez-Alonso, A.; Tascon, J. M. D. *Carbon* **2000**, *38*, 1183.
(36) Patrick, D. L.; Cee, V. J.; Beebe, T. P., Jr. *Science* **1994**, *265*, 231.
(37) Chen, A.; Kwon, S.; Borguet, E.; Vidic, R. *Proceedings of 25th Biannual Carbon Conference, Lexington, KY*; 2001.
(38) Atkins, P. W. *Physical Chemistry*, 5th ed.; W. H. Freeman and Company: New York, 1994.
(39) Krishna, S.; Gullett, B. K.; Jozewicz, W. *Environ. Sci. Technol.* **1994**, *28*, 1506.
(40) Bacon, R.; Tang, M. *Carbon* **1964**, *2*, 221.
(41) Li, Y. H.; Lee, C. W.; Gullett, B. K. *Carbon* **2002**, *40*, 65.
(42) Huggins, F. E.; Huffman, G. P.; Dunham, G. E.; Senior, C. L. *Energy Fuels* **1999**, *13*, 114.
(43) Cremer, P. S.; Su, X.; Somorjai, G. A.; Shen, Y. R. *J. Mol. Catal. A* **1998**, *131*, 225.

Received for review March 27, 2002. Revised manuscript received June 20, 2002. Accepted July 3, 2002.

ES0256818